Chapter 5

STUDIES ON $CuInS_2$ THIN FILMS PREPARED USING CHLORIDE AND NITRATE BASED PRECURSOR SOLUTIONS

5.1 Introduction

High conversion efficiency and low fabrication costs are the two principal requirements of thin film solar cells for terrestrial applications. Several promising materials are currently being investigated in an effort to improve properties and reduce process costs; $CuInS_2$ is particularly a promising candidate because of its optimum direct band gap (E_g = 1.5 eV) [1] and its controllable conversion type [2]. This is one of the I-III-VI_2 type semiconductors that crystallize in chalcopyrite structure. Thin film solar cells based on $CuInS_2$ have reached efficiency above 10% that make them a promising candidate for future energy requirements [3]. Wider band gap of $CuInS_2$ compared to other widely used chalcopyrites such as $CuInSe_2$ and $Cu(In,Ga)Se_2$ has an advantage of potentially higher open circuit voltages. It is also important that sulfur is less toxic than selenium. It has been predicted theoretically that homojunction fabricated using this material can yield an efficiency of 27 to 32% [4].

A variety of techniques have been applied to deposit $CuInS_2$ thin films [5-9] including molecular beam epitaxy, flash evaporation, r f sputtering, chemical vapor deposition and chemical spray pyrolysis (CSP). One of the major problems of this class of materials is the control of stoichiometry ie, control of the excess copper content and of the copper to indium and metal to chalcogen ratios. Because of the large difference in the vapor pressures of copper, indium and chalcogen, the stoichiometry is controlled by means of sophisticated vapor monitoring techniques. Unlike the case of physical vapor deposition techniques, in CSP technique, ratios of the constituents in the sample are directly linked to their concentrations in the spray solution. Hence this technique is ideally suited for deposition of large area films with

controlled stoichiometry and dopant profiles [10]. One can even think of varying stoichiometry along film thickness by making appropriate changes in molarity ratio of the solution.

Also, for economic reasons, it should be very interesting to deposit these films using a cheap deposition technique. In that case, spray pyrolysis appears very promising since $CuInS_2$ films with good crystalline properties were grown. In most of the cases $CuInS_2$ thin films were deposited from aqueous solution containing $CuCl_2$, $InCl_3$ and thiourea [11-14]. Pamplin et al prepared $CuInS_2$ thin films using cuprous chloride, cupric acetate and cupric chloride as sources of copper. It was also found that N, N-dimethyl thiourea gave better quality layers than those obtained from thiourea [15].

In this chapter, properties of $CuInS_2$ thin films prepared using chloride and nitrate based precursor solutions are described. Nitrate based precursor solutions were used to avoid formation of chlorine impurity phase in the films. There were no earlier reports on sample preparation using nitrate-based precursors. The structural and optical properties of sprayed films were determined mainly by growth temperature and Cu/In ratio in the spraying solution. We have obtained information about the dependence of the composition of the elements in the films as a function of the composition in the spray solution. Nitrate based $CuInS_2$ films showed better stoichiometry. It could be seen that chemical composition in the solution controlled film resistivity in a wide range, a fact that might be useful when designing solar cells made from this material. Crystallinity, photosensitivity and band gap of the samples are also important as far as solar cells are concerned. The surface morphology, structural and optical properties, depth analysis (XPS) and temperature dependent conductivity of both the set of samples are also discussed.

5.2 Experimental Details

$CuInS_2$ thin films were prepared using chloride and nitrate based precursor solutions using CSP. In the first case aqueous solutions of $CuCl_2$, $InCl_3$ and thiourea ($CS(NH_2)_2$) were used as the precursors, while in the second case $Cu(NO_3)_2$, In $(NO_3)_3$ and thiourea were used as precursors. Indium chloride was prepared by dissolving high purity indium (99.99%) in concentrated HCl and indium nitrate was prepared by dissolving the same in concentrated HNO_3. All the solutions were prepared in distilled water. 375 ml of the solution was sprayed onto glass substrates kept at 300°C. The maximum volume of the solution that could be sprayed in a single stretch for getting uniform good films without any pinholes was 375 ml. On further increasing the volume, it resulted in the development of pinholes in the sample. Thus in a single spray we could not increase the film thickness beyond a limit. Equal volumes of the solutions were mixed in appropriate molar concentrations to get different Cu/In ratios. Cu/In ratio was varied from 0.5 to 1.5 keeping S/Cu ratio at 5.For this, the molarity ratio of $CuCl_2$ (or $Cu(NO_3)_2$) and thiourea was kept at 0.0125 M and 0.0625 M respectively while molarity of $InCl_3$ (or $In(NO_3)_3$) was varied. Air was used as the carrier gas and the spray rate was kept at 20 ml/min in all cases. Samples prepared using chloride based precursor solution were named C1, C2, C3, C4 and C5 having Cu/In ratio 0.5. 0.7,1, 1.2 and 1.5 respectively, keeping S/Cu ratio at 5. For nitrate based precursor solutions samples were represented as N1, N2, N3, N4 and N5 having Cu/In ratio 0.5, 0.7, 1, 1.2 and 1.5 respectively with S/Cu ratio 5.

5.3 $CuInS_2$ from Chloride Based Precursor Solution

5.3.1 Structural Analysis

XRD spectrum of the samples is depicted in Fig 5.1. Crystallinity of the samples was found to increase with increase in Cu/In ratio. Four characteristic peaks corresponding to planes (112), (220), (312) and (224) appeared for sample C5 (JCPDS-270159) with preferential orientation along (112) plane. The improvement in

crystallinity when Cu/In ratio was increased was an effect, which had been attributed to copper mobility [16]. The *d* values and peak intensities are compared in Table 5.1. Peak corresponding to (220) plane of $CuInS_2$ indicated formation of $CuInS_2$ phase in both Cu-poor C1 and C2 samples. A broad peak with a shoulder was obtained for Cu-poor C1 sample at around 26.5° and another one at 64°. This might be due to some impurity phase formation in the sample. The diffraction peak at $2\theta = 26.5°$ could be related to the formation of In_2S_3 phase (JCPDS-330623), due to presence of excess indium as observed from EDAX analysis. Films with excess indium did not show good crystallinity due to the presence of secondary chemical phases of In_2S_3 and InS, and very likely due to the lattice deformation by copper vacancies being occupied by indium atoms. The peak at 64° corresponds to the formation of InS phase (JCPDS-190588).

Table 5.1 XRD data of $CuInS_2$ film

2θ (degrees)	d [Å] (observed)	d [Å] (standard)	hkl	I/I_0 (observed)	I/I_0 (standard)
27.91	3.1932	3.198	112	100	100
46.27	1.9603	1.952	220	10.54	10
54.88	1.6716	1.666	312	2.80	12
57.70	1.5962	1.601	224	16.51	4

Grain size was calculated from the Debye-Scherrer formula for samples C3, C4 and C5 since they only showed maximum intensity peak along the same plane. The value was found to increase from 5.8 nm to 21.23 nm with increase in the Cu/In ratio. Lattice parameters were calculated to be a = b = 5.54 Å and c = 11.01 Å which was in good agreement with the standard values of a = b = 5.523 Å and c = 11.141 Å.

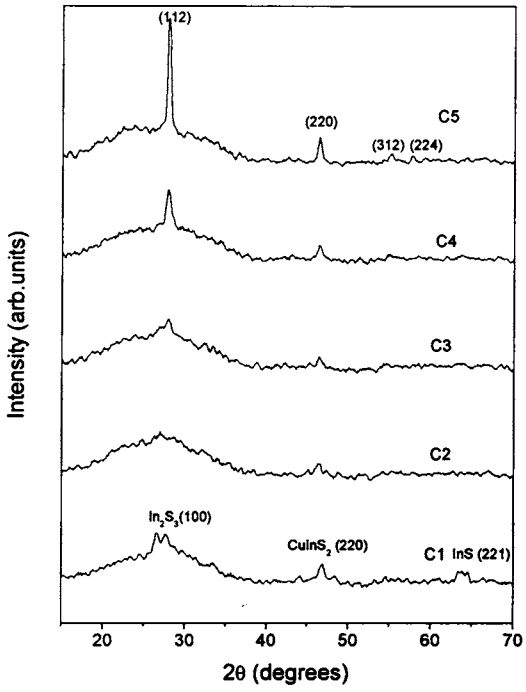

Fig. 5.1 XRD pattern of samples C1, C2, C3, C4 and C5

5.3.2 Surface Morphology

Surface morphology was examined using SEM. In-rich solutions produced films (C1) with smooth surface and small grains. SEM micrographs showed agglomerated areas in Cu-rich films. The number as well as size of the agglomerated area increased with increasing copper concentration in the solution. Chemical composition of the agglomerated area was different from composition of the flat region. The copper content in this area was higher than that in the flat region and indium content was essentially decreased [17]. SEM micrographs are compared in Fig.5.2 (a), (b) and (c).

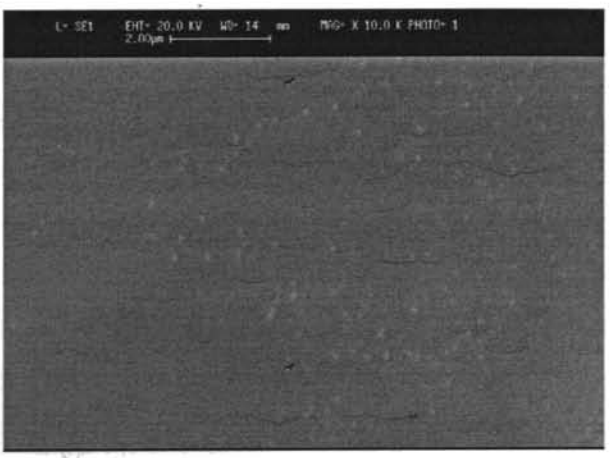
L= SE1 EHT= 20.0 KV WD= 14 mm MAG= X 10.0 K PHOTO= 1
2.00µm

(a)

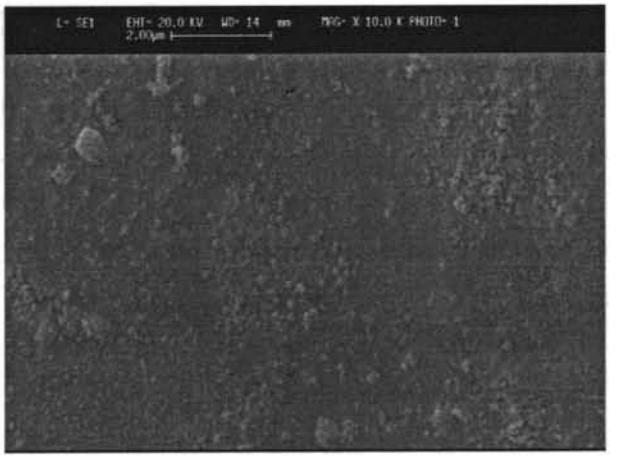
L= SE1 EHT= 20.0 KV WD= 14 mm MAG= X 10.0 K PHOTO= 1
2.00µm

(b)

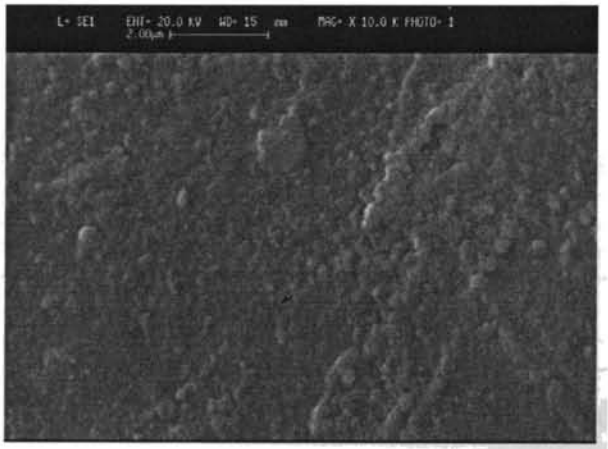

(c)

Fig. 5.2 Surface morphology (a) C1 (b) C4 (c) C5

5.3.3 EDAX Measurements

Composition of $CuInS_2$ films was studied using EDAX measurements. Atomic concentration of Cu, In and S in the film is compared in Table 5.2.Cu/In and S/Cu ratios were found to be always less than that taken in the solution. The EDAX spectrum of sample C1 is shown in Fig.5.3.

Table 5.2 Atomic concentrations of Cu, In and S

Sample	Cu (%)	In (%)	S (%)	Cu/In ratio in film
C1 (Cu/In = 0.5)	11.27	25.65	54.52	0.44
C3 (Cu/In = 1.0)	16.36	23.75	56.33	0.69
C4 (Cu/In = 1.2)	15.47	16.68	59.12	0.93
C5 (Cu/In = 1.5)	15.72	12.58	59.08	1.25

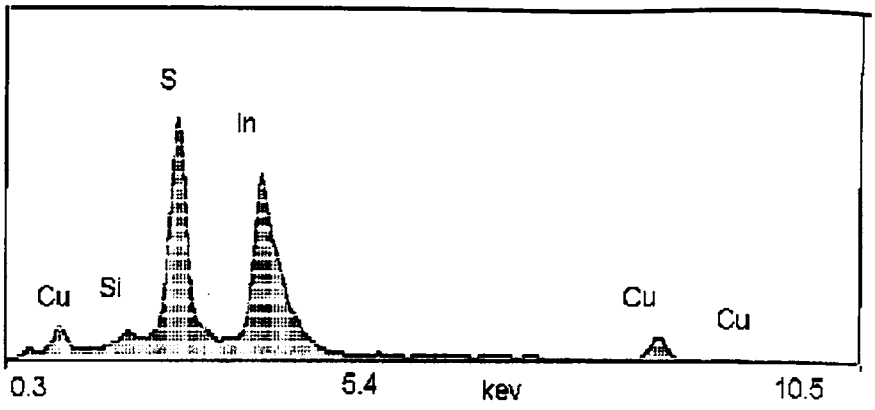

Fig. 5.3 EDAX spectrum of sample C1

5.3.4 XPS Analysis

In order to know the chemical state of the elements along the thickness of the samples, we performed XPS depth profile of the samples. Here the presence of the elements Cu, In, S, O and Si was checked along the thickness of the samples. It could be seen that all the elements diffused slightly into the glass substrate, probably due to the high temperature at which spraying was done. Oxygen was present only at the surface of these samples. This was very much evident in Fig.5.4 (a) and (b). The BE value of surface oxygen was found to be 532 eV, which was due to surface contamination [18]. BE values of Cu, In and S indicated formation of $CuInS_2$ and these are compared in Table 5.3. Interestingly chlorine was absent in these samples.

Table 5.3 BE value of Cu, In and S as observed from XPS Analysis

Element	Binding Energy (eV)
$Cu2p_{3/2}$	932.5
$Cu2p_{1/2}$	952.5
$In3d_{5/2}$	444.7
$In3d_{3/2}$	452.7
S2p	162.0

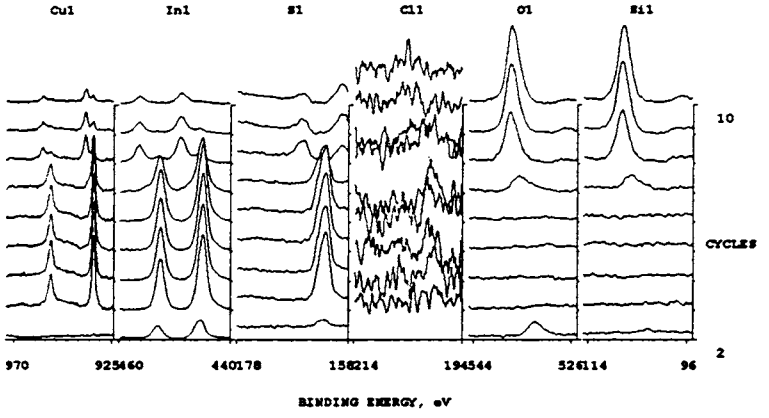

(a)

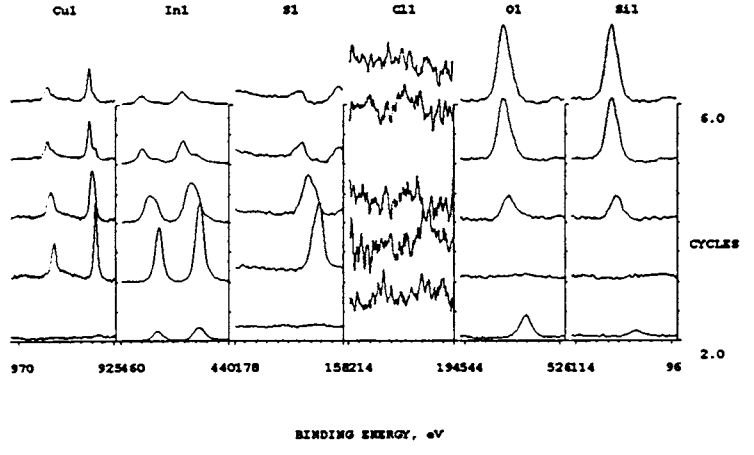

(b)

Fig. 5.4 Depth profile of sample (a) C1 (b) C5

5.3.5 Optical Studies

We obtained band gap from the plot of $(\alpha h\nu)^2$ vs hν [Fig.5.5] and was found to decrease from 1.51 eV to 1.32 eV for sample C1 to C5 [Fig.5.6]. This variation was in accordance with the variation in crystallinity of the samples as observed from XRD [Fig. 5.1]. Another possible cause for this effect might be carrier degeneracy in $CuInS_2$ due to defects in the crystal lattice [12] and/or due to the increase in Cu/In ratio. This was evident from the high conductivity of sample C5.

Transmittance spectra of the samples in the wavelength range 400 – 1200 nm are shown in Fig.5.7. Percentage of transmittance was found to decrease with increase in Cu/In ratio.

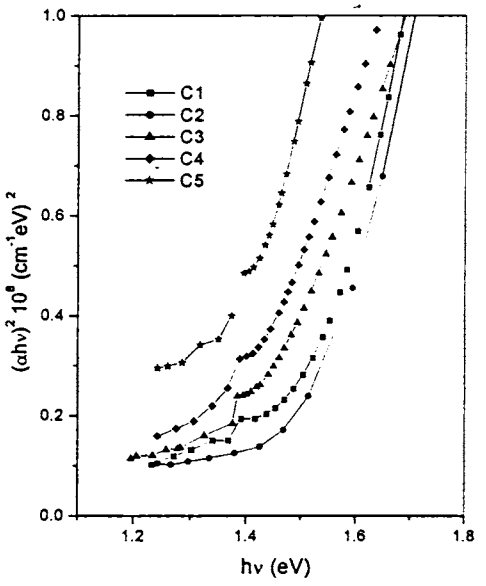

Fig.5.5 $(\alpha h\nu)^2$ vs hν for samples C1 to C5

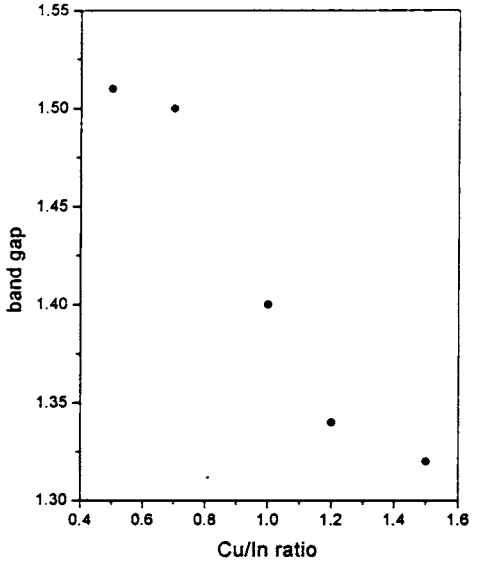

Fig. 5.6 Variation in band gap (C1 to C5)

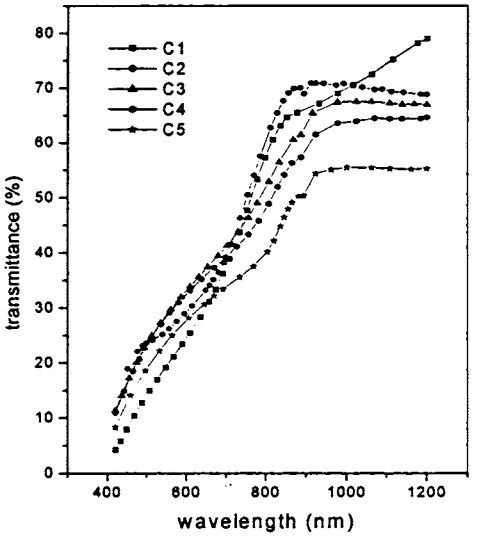

Fig. 5.7 Wavelength dependence of transmittance for samples C1 to C5

5.3.6 Photosensitivity Measurements

Figure 5.8 shows variation in photosensitivity with Cu/In ratio. The value decreased drastically with increase in the Cu/In ratio. Thus the sample C1 was found to have maximum photoresponse. High resistivity of sample C1 indicated a reduction in the number of majority carriers. So, probably the minority carriers, surviving to contribute to photoconductivity for this sample might be more, indicating high photosensitivity.

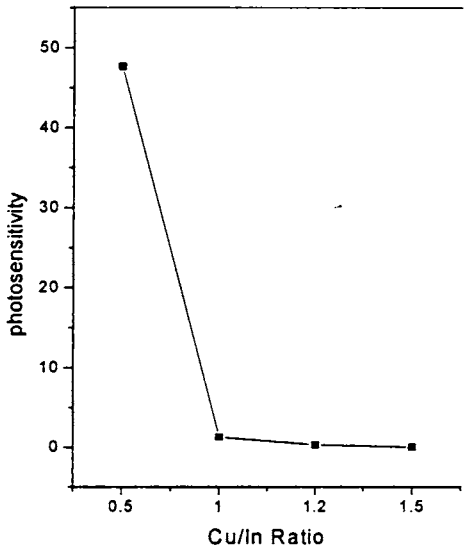

Fig.5.8 Variation in photosensitivity with Cu/In ratio

5.4 $CuInS_2$ from Nitrate Based Precursor Solution

5.4.1 Structural Analysis

It was obvious from the XRD spectra that the crystallinity of the samples increased with increase in Cu/In ratio [Fig.5.9]. All the samples showed preferential orientation along (112) plane. Cu-poor nitrate based $CuInS_2$ films seem to be more crystalline when compared to that of samples prepared from chloride based solutions. Grain sizes are compared in Fig.5.10. Grain size increased from 6.64 nm for N1

(Cu/In=0.5) to 20.6 nm for N5 (Cu/In=1.5). Thus the grain size was found to depend on the content of copper and indium in the films.

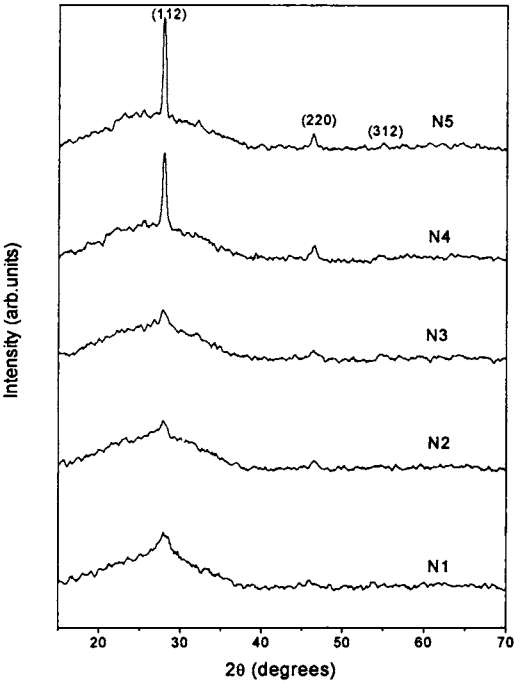

Fig. 5.9 XRD pattern of samples N1 to N5

5.4.2 Surface Morphology

$CuInS_2$ layer was characterized by means of scanning electron microscopy (JEOL Scanning Microscope Model JSM-8404) for surface observation. No surface feature was observed in the film and the film appeared to be uniform. This improved on increasing Cu/In ratio. SEM micrographs of samples N1 and N4 are shown in Fig. 5.11 (a) and (b). Both Cu-rich and In-rich films had fairly smooth structure, consisting of non-featured grains.

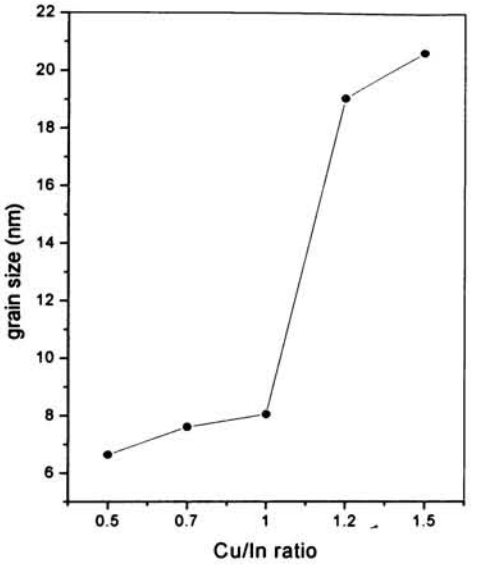

Fig. 5.10 Grain sizes of nitrate based $CuInS_2$ films

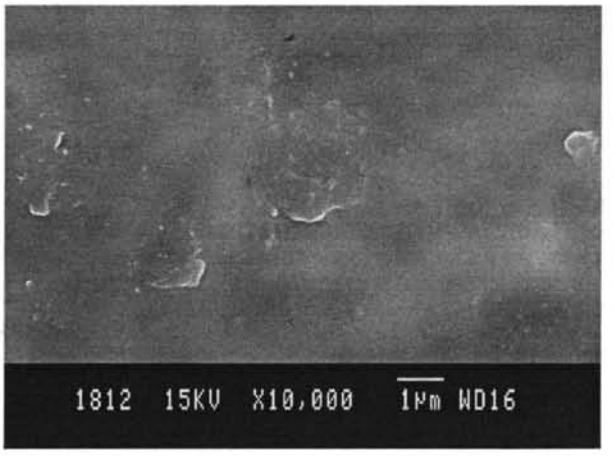

(a)

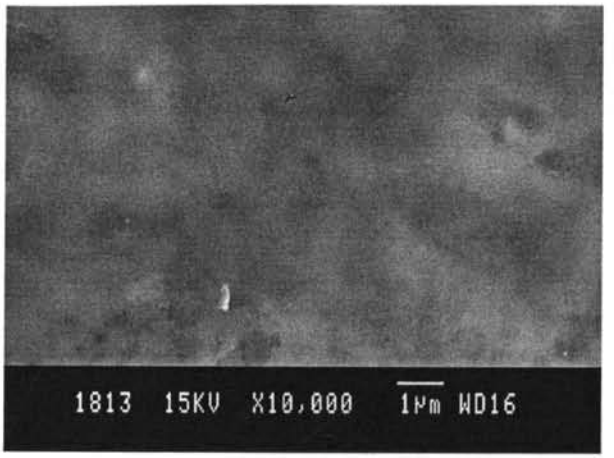

(b)

Fig. 5.11 SEM micrographs of samples (a) N1 and (b) N4

5.4.3 EDAX Measurements

Chemical composition of the samples was determined with EDAX measurements [Oxford systems, Model 6211 attached to JEOL Scanning Microscope (JSM-840A)]. Cu/In ratio followed the variation that had been made in the solution [Table 5.3]. Samples were found to be more stoichiometric when compared to that of chloride based films. Moreover Cu/In ratio in the sample was almost equal to that of the solution. This did not happen in the case of samples C1-C5.

Table 5.3 Variation in atomic concentration as observed from EDAX measurements

Sample	Cu (%)	In (%)	S (%)	Cu/In ratio in film
N1 (Cu/In = 0.5)	15.49	32.09	52.42	0.48
N3 (Cu/In = 1.0)	22.75	25.16	52.09	0.91
N4 (Cu/In = 1.2)	26.26	21.43	52.31	1.23

EDAX spectrum for samples N1 and N4 are given in Fig.5.12 (a) and (b). From the spectrum it was observed that the concentration of indium was high in sample N1 compared to sample N4.

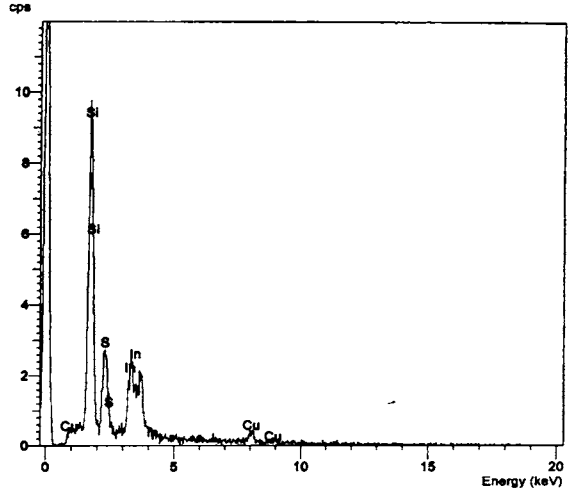

(a)

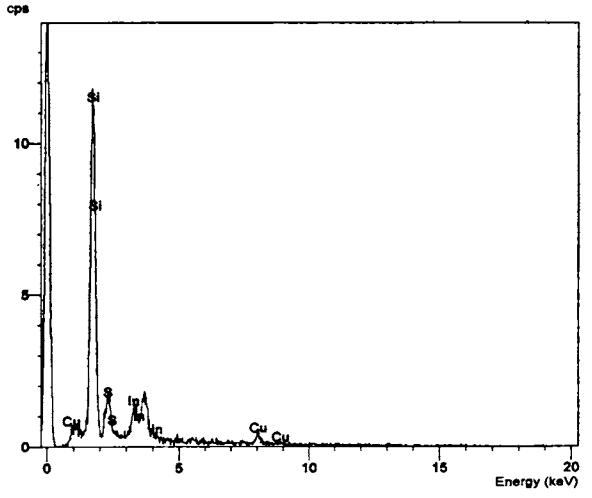

(b)

Fig. 5.12 EDAX spectrum of sample (a) N1 (b) N4

5.4.4 XPS Analysis

BE values of 932.5 eV, 952.5 eV, 444.74 eV, 452.7 eV and 162 eV for $Cu2p_{3/2}$, $Cu2p_{1/2}$, $In3d_{5/2}$, $In3d_{3/2}$ and S2p indicated formation of $CuInS_2$. Depth analysis of samples N1 and N3 are given in Fig. 5.13 (a) and (b) respectively.

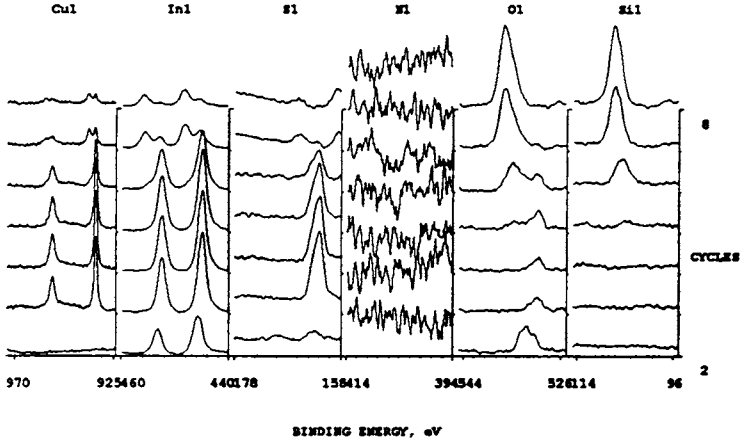

(a)

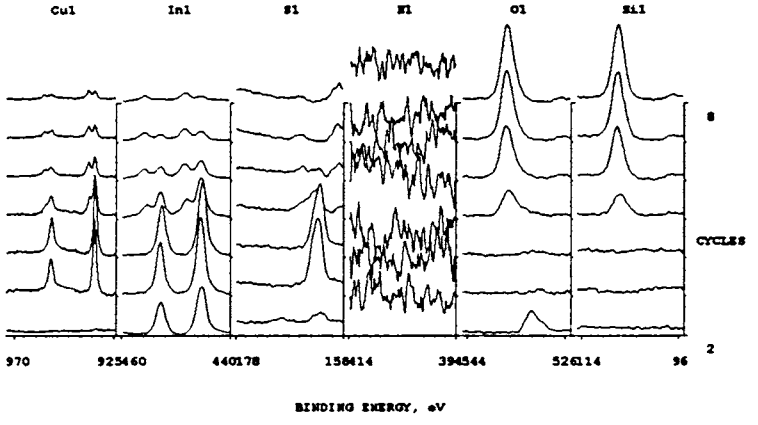

(b)

Fig. 5.13 Depth analysis of samples (a) N1 (Cu/In=0.5) (b) N3 (Cu/In=1)

Cu, In and S were uniformly distributed along the depth of the samples. BE peak at 532 eV of oxygen at the surface corresponds to surface contamination of the samples. Unlike in the case of sample C1 here in N1 oxygen was present throughout the depth of the sample, indicating that oxygen was not only chemisorbed on the surface, but oxygen-containing phase was formed during film growth. The binding energy of oxygen in the bulk (530 eV) corresponds to that of indium oxides (529.8 eV-530.5 eV for O 1s in In_2O_3). But as the film become stoichiometric, we could not observe any oxygen in the bulk of the sample (N3). Moreover nitrogen or its oxides were also not present in any of these samples.

5.4.5 Optical Studies

Band gap was found to be decreasing with increase in Cu/In ratio. The value decreased from 1.44 eV for sample N1 to 1.3 eV for sample N5. $(\alpha h\nu)^2$ vs hν plot for the samples are shown in Fig. 5.14. The percentage of transmittance decreased with increase in Cu/In ratio in the wavelength range 400 nm-1200 nm [Fig.5.15].

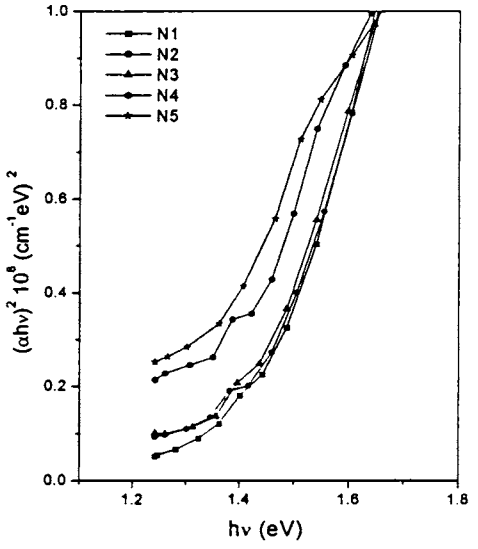

Fig. 5.14 Variation of band gap with Cu/In ratio

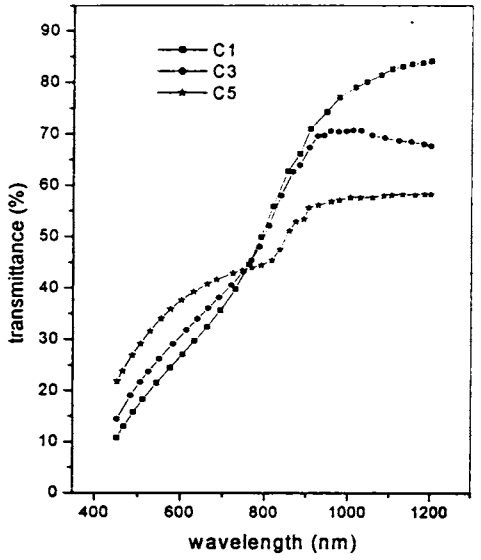

Fig. 5.15 Transmittance spectra of samples N1, N3 and N5

5.4.6 Photosensitivity Measurements

Photosensitivity of nitrate-based samples was found to be less than that of chloride-based samples except for sample N5. Sample N5 was found to be less conducting compared to sample C5. Here the number of majority carriers was less, and hence more minority carriers might be surviving to contribute to sensitivity. High sensitivity of sample C1 in comparison with N1 might be due to the presence of photosensitive In_2S_3 phase [19] as observed from XRD [Fig.5.1].

Here the maximum value of photosensitivity was found to be 18.9. But in the case of chloride sample this was 47.7. Similar observation was made in In_2S_3 prepared from chloride and nitrate precursor solutions. Fig. 5.16 depicts variation in photosensitivity with Cu/In ratio. When copper concentration was increased, naturally majority carrier concentration in the sample increased and hence minority carrier concentration will be decreased leading to decrease in photosensitivity.

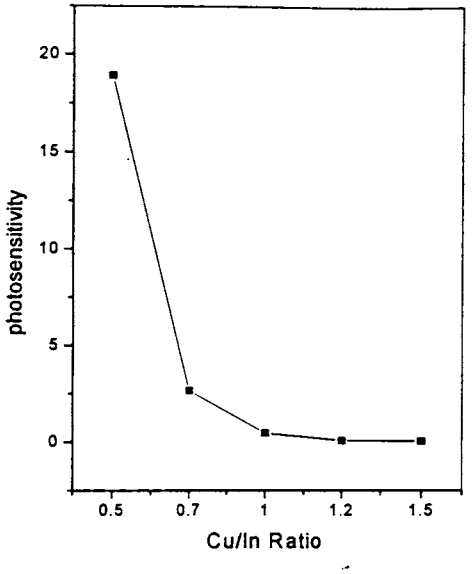

Fig. 5.16 Variation in photosensitivity with Cu/In ratio

5.5 Temperature Dependent Conductivity of Chloride and Nitrate Based $CuInS_2$ Films

Temperature dependent conductivity measurements in the temperature range 100 K- 300 K for both chloride and nitrate based samples (C1, C3, C5 and N1, N3, N5) were done using liquid helium cryostat having autotuning temperature controller (Lakeshore 321 model). Current and voltage were measured using a source measure unit (SMU) (Model: Keithley 236) interfaced by GPIB card and ICS software. Electrical contacts were given using silver paste painted on the surface of the sample at a separation of 0.5 cm.

Conductivity of the samples was found to increase with increase in Cu/In ratio. Of all the samples, N1 was highly resistive (more than C1), and this might be due to the high indium content in the sample as observed from EDAX [Table 5.3]. In fact indium rich samples (C1 and N1) were found to be n-type from Hot Probe

measurements. The high resistivity of indium rich films (C1 and N1) could also be due to poor crystallinity of these samples [Fig.5.1 and Fig. 5.9]. But on increasing Cu/In ratio, sample N3 was found to be more conducting compared to C3 and the samples were p-type. Sample N3 maintained better stoichiometry (in the film, EDAX) than sample C3. Conductivity values at room temperature are compared in Table 5.4.

Table 5.4 Comparison of conductivity at room temperature

Chloride	σ $(\Omega\text{-cm})^{-1}$	Nitrate	σ $(\Omega\text{-cm})^{-1}$
C1	3.78×10^{-6}	N1	6.40×10^{-7}
C3	3.88×10^{-5}	N3	1.98×10^{-4}
C5	15.86	N5	5.65

Log ρ versus Cu/In ratio for films grown from chloride and nitrate based precursor solutions are shown in Fig.5.17. From the graph it was clear that the film resistivity showed a big decrease of around seven orders of magnitude when the Cu/In ratio was increased from 0.5 to 1.5.These results indicated that excess copper caused hole degeneracy in the deposited films. Moreover the ratio Cu/In was found to have an important role in controlling the electrical properties of the $CuInS_2$ films. Interestingly this ratio could be easily controlled in samples prepared using CSP technique by adjusting molarity ratio in the spray solution.

From the Arrhenius plot of conductivity, samples C3 and N3 were having comparable activation energies and C5 and N5 exhibited low activation energies. Combining the results of electrical and stoichiometric analysis, the energy levels of the defects could be identified. The $\ln\sigma$ vs 1000/T graph for sample C1 is shown in Fig.5.18.

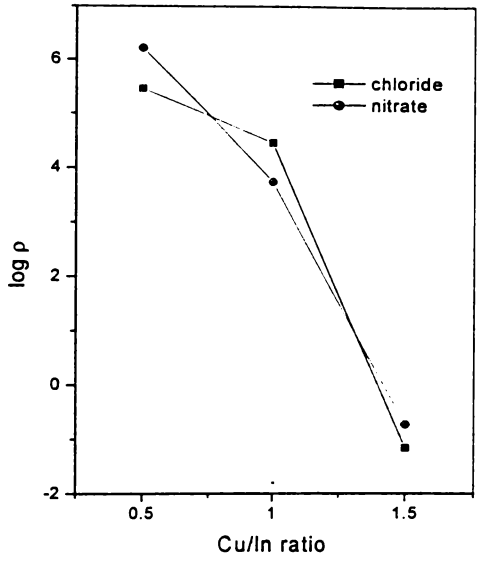

Fig 5.17 log ρ vs Cu/In ratio for chloride and nitrate based films

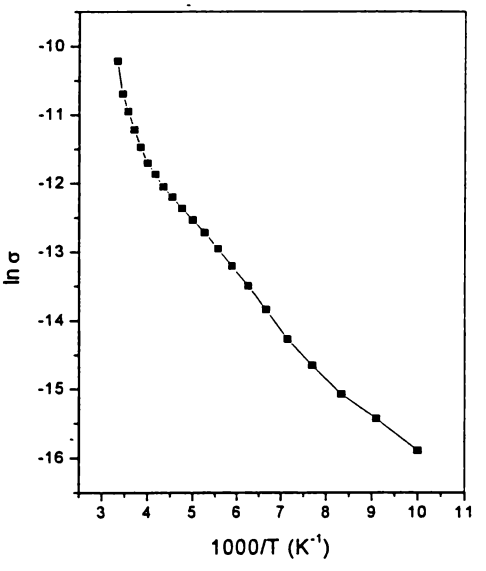

Fig. 5.18 Arrhenius plot of sample C1

For sample C1 we could identify three defect levels corresponding to activation energies 183.5 meV, 66.4 meV and 48.2 meV. From the EDAX measurements, indium was found to be in excess for sample C1. Thus the donor level at 183.5 meV could be ascribed to In at the interstitial position (In_i, 180 meV) [20]. Moreover the sample showed n-type conductivity, which also supported the existence of this level. Other two activation energies (66.4 meV and 48.2 meV- donor levels) were so close to each other, and might be due to indium occupying copper vacancy In_{Cu} (75 meV and 35 meV) [20, 21]. This level also might be contributing to the n-type conductivity of the sample. Indium sulfide (n-type) phase was also observed in the sample [Fig. 5.1]. Atomic concentration of indium was very high for sample N1 compared to C1 and thus it showed high resistivity. In fact we were unable to take conductivity measurements at low temperature because of high resistivity.

For samples C3 and N3 also, we could identify three defect levels corresponding to 189 meV, 125.6 meV and 6 meV and 183 meV, 123 meV and 6.7 meV respectively. Arrhenius plot for samples C3 and N3 are shown in Fig. 5.19 (a) and (b).

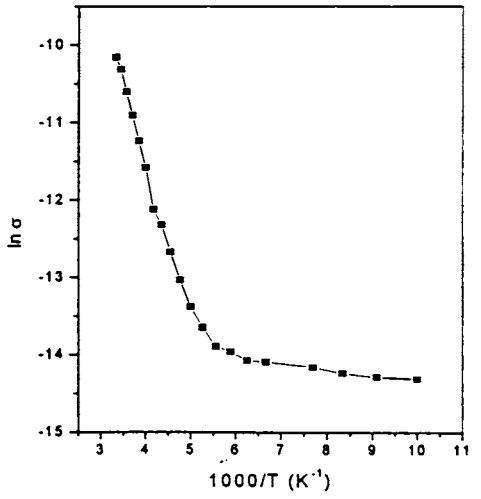

(a)

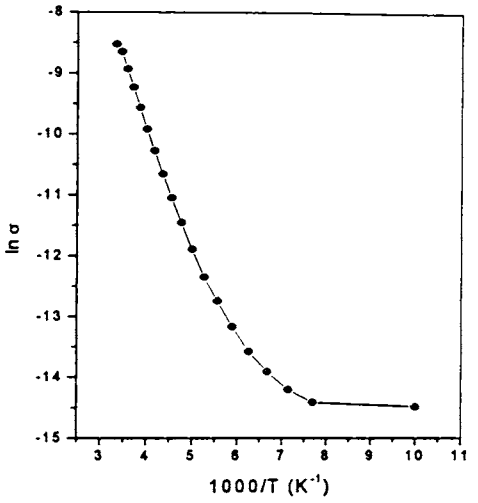

(b)

Fig.5.19 Arrhenius plots for (a) C3 (b) N3

Here the samples showed p-type conductivity and were found to have excess sulfur (>50%) and thus the level at ~180 meV (above the valence band) could be arising due to sulfur at the interstitial position (S_i) [22]. The level at ~120 meV could be linked to vacancy of Cu (V_{Cu}) which is the most probable defect in a sample having excess indium [23]. This is an acceptor level. The level corresponding to activation energy of ~ 6 meV might be contributing to conductivity, as samples C3 and N3 were found to have better conductivity compared to C1 and N1. The observed slopes (C3 and N3) were always increasing with temperature, which was compatible with grain boundary scattering mechanisms [24]. The classical grain boundary trapping theory assumes the presence of trapping states at the grain boundaries, which capture free carriers. These charged states at the grain boundaries create depleted regions and potential barriers, which provide a resistance to the passage of carriers from a grain to a neighboring one.

Temperature dependent conductivity measurements for samples C5 and N5 are given in Fig. 5.20 (a) and (b). It was very clear from the graph that the conductivity of the samples increased linearly with temperature even from low temperature itself.

We could identify only shallow levels 2.3 meV, 0.81 meV and 0.17 meV for sample C5 and 8.7 meV, 3.4 meV and 1.4 meV for sample N5. Samples C5 and N5 were highly conducting in comparison to the other samples (C1, N1 and C3, N3). Thus these shallow levels might be contributing to the conductivity of the samples.

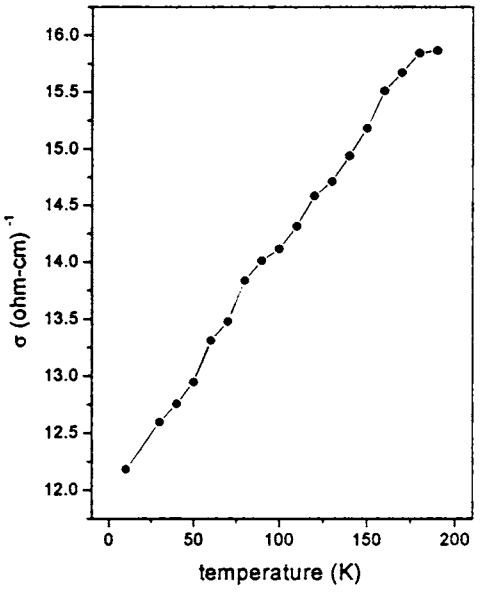

(a)

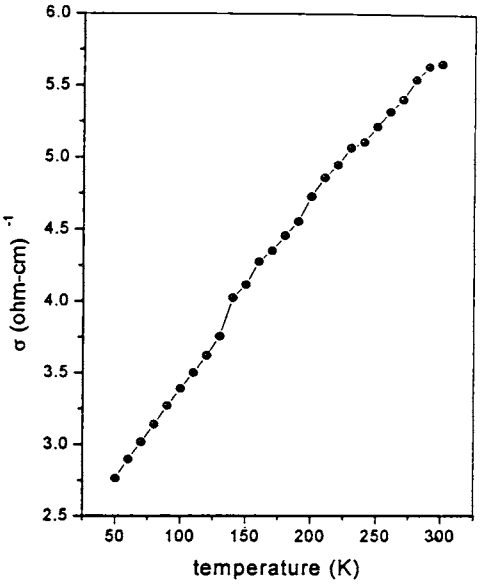

(b)

Fig. 5.20 Temperature dependent conductivity for samples (a) C5 (b) N5

5.6 Conclusion

$CuInS_2$ thin films were prepared using chloride and nitrate based precursor solutions. In single spray we could not increase volume of the solution beyond 375 ml as the film got damaged. Nitrate based $CuInS_2$ samples showed better crystalline structure and better stoichiometry in comparison. The band gap of the samples decreased with increase in Cu/In ratio in both cases. BE values from XPS studies indicated formation of $CuInS_2$.Conductivity of both set of samples increased with increase in Cu/In ratio. Chloride based samples showed better photosensitivity for Cu poor samples (but n-type), but for samples having higher Cu/In ratio photosensitivity decreased drastically. Nitrate based samples show better crystallinity, stoichiometry, conductivity (N3) and a slightly low photosensitivity. These samples may show better

characteristics if they are used for fabricating solar cells. Defect levels were identified using the temperature dependent conductivity measurements and composition analysis. It is worth mentioning here that there are no publication giving results of similar studies in this material, to the best of our knowledge. Through this study we could establish that in CSP technique one can control electrical properties by adjusting molarity ratio of spray solution. Another important point was that Cu/In ratio was the controlling parameter as far as the electrical properties of the film was concerned. Major difficulty we observed was the preparation of thick films. We could not spray large volume of solution (> 375 ml) at a single stretch. This has to be solved.

References

[1] J. L. Shay and J. H. Wernick *Ternary Chalcopyrite Semiconductors: Growth, Electronic Properties and Applications*, Pergamon Press, New York (1975)

[2] D. C. Look and J. C. Manthuruthil *J. Phys. Chem. Solids* **37** (1976) 173

[3] J. Klaer, J. Bruns, R. Henninger, K. Siemer, R. Klenk, K. Ellmer and D. Bräunig *Semicond. Sci. Technol.* **13** (1998) 1456

[4] J. M. Meese, J. C. Manthuruthil and D. R. Locker *Bull.Amer.Phys.Soc.* **20** (1975) 696

[5] F. R. White, A. H. Clark, M. C. Grey and L. L. Kazmerski *J. Appl. Phys.* **50** (1979) 544

[6] H. L. Hwang, C. C. Tu, J. S. Maa and C. Y. Sun *Sol. Energy Mater.* **2** (1980) 433

[7] H. L. Hwang, C. L. Cheng, L. M. Liu and C. Y. Sun *Thin Solid Films* **67** (1980) 83

[8] S. P. Gindle, C. W. Smith and S. D. Mittlem *Appl. Phys. Lett.* **35** (1979) 24

[9] H. Bihri and M. Abd-Lefdil *Thin Solid Films* **354** (1999) 5

[10] A. N. Tiwari, D. K. Pandya and K. L. Chopra *Thin Solid Films* **130** (1985) 217

[11] H. Bihri, C. Messaoudi, D. Soyah, A. Boyer, A. Mzerd and M. Abd-Lefdil *Phys. Stat. Sol. (a)* **129** (1992) 193

[12] M. Ortega-Lopez and A. Morales-Acevedo *Thin Solid films* **330** (1998) 96

[13] M. Krunks, O. Bijakina, V. Mikli, H. Rebane, T. Varema, M. Altosaar and E. Mellikov *Sol. Energy Mater. Sol. Cells* **69** (2001) 93

[14] J. González-Hernández, P. M. Gorley, P. P. Horley, O. M. Vartsabyuk and Yu V. Vorobiev *Thin Solid Films* **403-404** (2002) 471

[15] B. Pamplin and R. S. Feigelson *Thin Solid Films* **60** (1979) 141

[16] R. Klenk, T. Walter, H. W. Schock and D. Cahen *Adv. Mater.* **5** (1993) 114

[17] M. Krunks, V. Mikli, O. Bijakina and E. Mellikov *Appl. Surf. Sci.* **142** (1999) 256

[18] Teny Theresa John, K. C. Wilson, P. M. Ratheesh Kumar, C. Sudha Kartha, K.P. Vijayakumar, Y. Kashiwaba, T. Abe and Y. Yasuhiro *Phys. Stat. Sol. (a)*

202 (1) (2005) 79

[19] Teny Theresa John, S. Bini, Y. Kashiwaba, T. Abe, Y. Yasuhiro, C. Sudha Kartha and K. P. Vijayakumar *Semicond. Sci. Technol.* **18** (2003) 491

[20] J. H. Schön and E. Bucher *Phys. Stat. Sol. (a)* **171** (1999) 511

[21] I. A. Aksenov, N. A. Sobolev and V. A. Sheraukhov *Phys. Stat. Sol. (a)* **123** (1991) K171

[22] H. J. Lewerenz *Sol. Energy Mater. Sol. Cells* **83** (2004) 395

[23] J. J. M. Binsma, L. J. Giling and J. Bloem *J. Lumin.* **27** (1982) 35

[24] S. Marsillac, M. C. Zouaghi, J. C. Bernède, T. Ben Nasrallah and S. Belgacem *Sol. Energy Mater. Sol. Cells* **76 (2)** (2003) 125